

# Results of the simulations of the petal/lens as part of the LAUE project

V. Valsan<sup>a,b</sup>, F. Frontera<sup>a</sup>, E. Virgilli<sup>a</sup>, V. Liccardo<sup>a,b</sup>, E. Caroli<sup>c</sup>, J.B. Stephen<sup>c</sup>

<sup>a</sup> *Physics and Earth Science Department, University of Ferrara, Via Saragat 1, 44122 Ferrara, Italy;*

<sup>b</sup> *Université de Nice Sophia-Antipolis, Parc Valrose, 06108 Nice Cedex 2, France;*

<sup>c</sup> *IASF-INAF via P.Gobetti, Bologna - Italy.*

## ABSTRACT

In the context of the LAUE project for focusing hard X-/gamma rays, a petal of the complete lens is being assembled at the LARIX facility in the Department of Physics and Earth Science of the University of Ferrara. The lens petal structure is composed of bent Germanium and Gallium Arsenide crystals in transmission geometry. We present the expectations derived from a mathematical model of the lens petal. The extension of the model for the complete LAUE project in the 90 – 600 keV energy range will be discussed as well. A quantitative analysis of the results of these simulations is also presented.

**Keywords:** Laue lenses, Focusing telescopes, Gamma-rays, X-ray instrumentation, Astrophysics.

## 1. INTRODUCTION

We propose a Laue lens<sup>1</sup> as a new focusing instrument in the soft gamma-ray band (80–600 keV) in order to answer most of the unresolved scientific open issues in soft gamma-ray astronomy.<sup>2</sup> (For an exhaustive review of Laue lenses see Ref. [3]). Lens prototypes have already been successfully built in the LARIX facility<sup>4</sup> of the University of Ferrara.<sup>5–8</sup> Preliminary simulation results of a petal made with Ge(111) and GaAs(111) was reported in [9]. The petal that is being built is made up of both GaAs(220) and Ge(111) crystal tiles.<sup>2,10,11</sup> The selection of the crystals and their characterization is presented in [12]. Here we report the final simulation and performance results of this lens petal and of a lens made of petals like that is being assembled of either Ge(111) or GaAs(220).

## 2. MODELLING THE PETAL STRUCTURE

The petal structure is modeled in such a way as to diffract photons in the energy band of 90 keV – 304 keV. This pass band is the actual energy band of the photons currently available in the LARIX facility. The crystals will be positioned and glued on the structure so as to focus the diffracted beam at a distance of 20 meters. Figure 1 illustrates the petal structure and also the respective positions of each crystal tile. Table 1 shows main parameters of this petal.

## 3. SIMULATING THE PETAL PSF

The Point Spread Function (PSF) gives the spatial distribution of the reflected photons in the focal plane when a point source at infinity is incident over the lens or petal.

The resulting PSF has been simulated taking into account all types of misalignment and distortion effects of every single crystal. A slight misalignment of a crystal from its nominal position creates a distortion in the PSF, therefore a precise positioning of each single crystal on the lens is crucial.

Another factor which affects the PSF is the distortion in the curvature of the crystals. The petal will be made of GaAs(220) and Ge(111) crystals curved with a radius of 40 meter. Any distortion in the curvature radius will also affect the PSF. The lens petal which has been simulated, is separately made up of Ge(111) and GaAs(220) crystal tiles, with an energy passband from ~90 keV to ~300 keV.

---

Send correspondence to:

valsan@fe.infn.it, frontera@fe.infn.it, virgilli@fe.infn.it, liccardo@fe.infn.it

Parameter	Value		
	section of GaAs(220)	section of Ge(111)	Entire petal
Focal length	20 meters	20 meters	20 meters
Energy range	148 – 304 keV	90 – 267 keV	90 – 304 keV
No. of Rings	14	18	18
Innermost radius	40.66 cm	28.40 cm	28.40 cm
Outermost radius	83.47 cm	83.47 cm	83.47 cm
No. of crystal tiles	119	155	274
Crystal size	$30 \times 10 \times 2 \text{ mm}^3$	$30 \times 10 \times 2 \text{ mm}^3$	$30 \times 10 \times 2 \text{ mm}^3$
Crystal mass (total)	$2.5 \text{ g} \times 119 = 297.5 \text{ g}$	$2.07 \text{ g} \times 155 = 320.85 \text{ g}$	618.35 g

Table 1. Parameters of the petal that is being build in the LARIX facility.

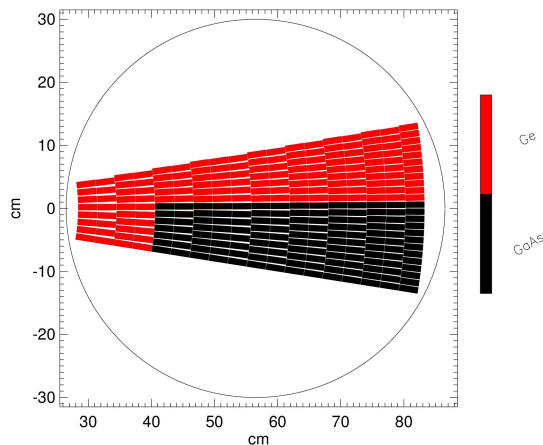


Figure 1. An illustration of the petal structure (that is being build in the LARIX facility) and the position of each crystal tile over it.

We have simulated the petal PSF assuming either bent crystal tiles made of GaAs (220) or bent crystal tiles made of Ge(111). The corresponding pass band is either 89–308 keV or 88–290 keV, respectively. The resulting PSF is shown in Figs. 2 and 3 in the case of GaAs(220) as the crystal tiles, and in Figs. 4 and 5 in the case of Ge (111). Figure 2 (in case of GaAs(220)) and Fig. 4 (in case of Ge(111)) show the PSF when the crystal tiles have no radial distortion and are positioned perfectly over the petal frame without any misalignment. On the other side, Fig. 3 and Fig.5, respectively for the case of GaAs(220) and Ge(111), show the resulting PSF when the crystal tiles have a radial distortion of 6 m (from the required 40 m) and are positioned over the petal frame with a misalignment of 30 arcsec. The main parameters of the simulated petals are given in Table 2.

### 3.1 Effect of the beam divergence

A Laue lens for astrophysical observations is built assuming that the incoming X-rays are parallel and paraxial. However, in laboratory, it is not possible to achieve this beam configuration given the finite distance between source and lens, and to the finite dimension of the source that has a radius of 0.4 mm. In order to minimize the beam divergence, a Tungsten bar 20 mm thick with a hole of 3 mm diameter and a lead bar 50 mm thick with a hole of 1 mm diameter are placed at the exit window of the X-ray source. The output beam, at a distance of 24.38 m, is further collimated with a second lead bar, which has in its center a Tungsten slit 20 mm thick with variable aperture  $S_w$ . After passing through this slit, the beam is incident on the crystal tile, which then

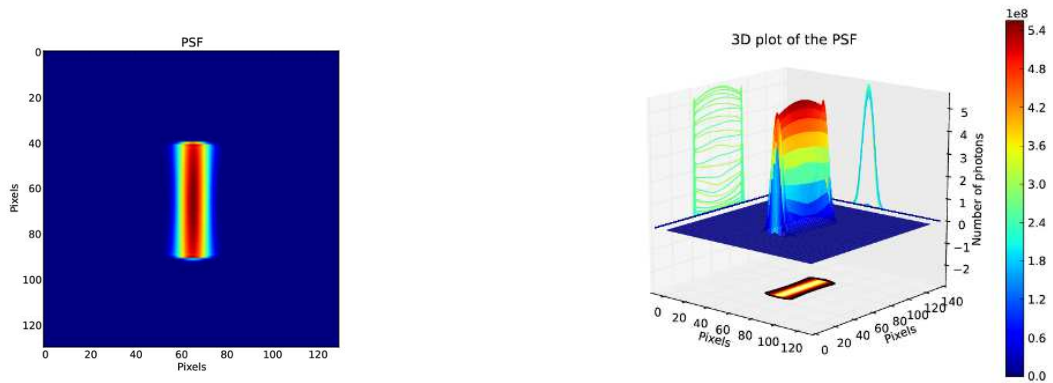


Figure 2. PSF of the petal made with GaAs(220) without any misalignment errors in the positioning of the crystal tiles having no radial distortion.

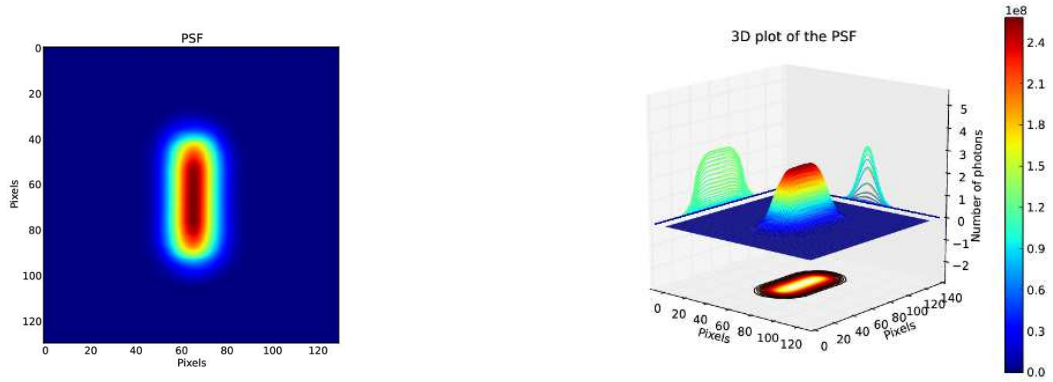


Figure 3. PSF of the petal made with GaAs(220) with a maximum misalignment of 30 arcsec in the positioning of the crystal tiles having a maximum radial distortion of 6 meters.

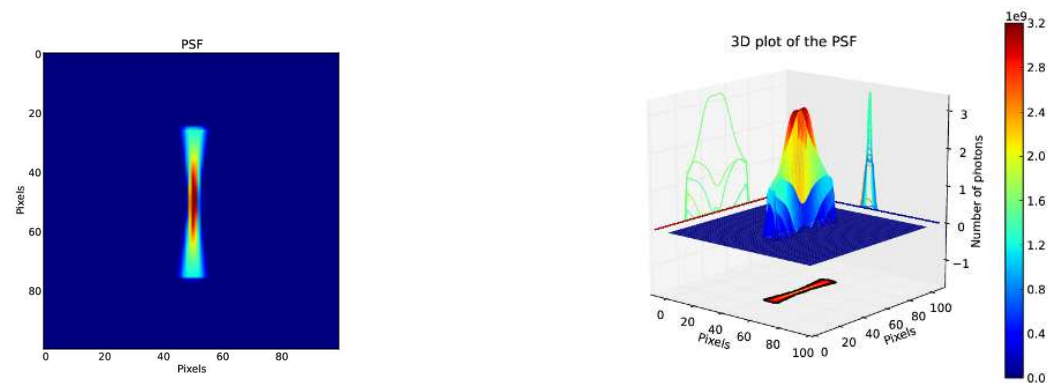


Figure 4. PSF of the petal made with Ge(111) without any misalignment errors in the positioning of the crystal tiles having no radial distortion.

diffraction and forms an image on the focal plane at a distance 20 meter from the crystal tile. The dependence of the Full Width at Half Maximum (FWHM) of the PSF on the slit width  $S_w$  is plotted in Fig. 6.

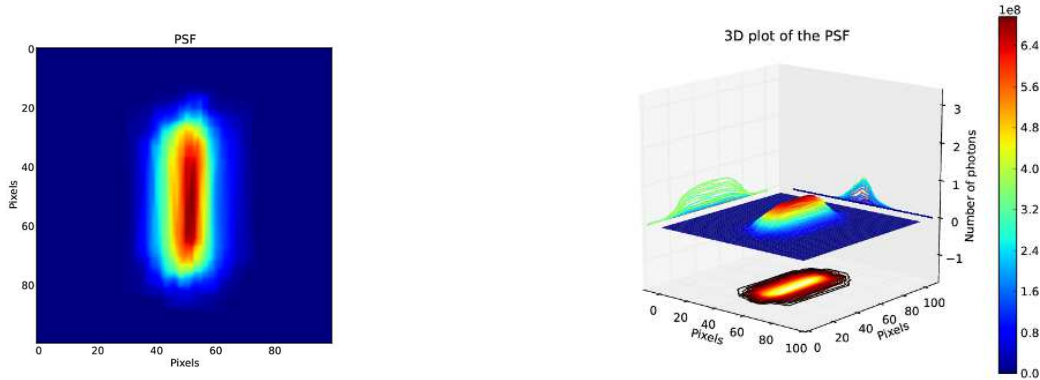


Figure 5. PSF of the petal made with Ge(111) with a maximum misalignment of 30 arcsec in the positioning of the crystal tiles having a maximum radial distortion of 6 meters.

Parameter	Value	
	case of GaAs(220)	case of Ge(111)
Focal length	20 meters	20 meters
Energy range	89 - 308keV	88 - 290keV
Subtended angle	18	18
No. of Rings	33	20
Innermost radius	41.71 cm	27.67 cm
Outermost radius	137.71 cm	84.67 cm
No. of crystal tiles	913	343
Crystal dimension	$30 \times 10 \times 2 \text{ mm}^3$	$30 \times 10 \times 2 \text{ mm}^3$
Crystal mass (total)	$2.5 \text{ g} \times 913 = 2282.5 \text{ g}$	$2.07 \text{ g} \times 343 = 710 \text{ g}$

Table 2. Parameters of the simulated petal.

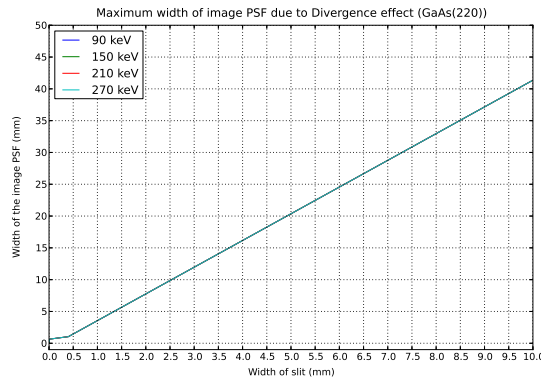


Figure 6. The effect of the divergence with the varying slit width (on the  $x - axis$ ) on the FWHM of the image PSF.

#### 4. SIMULATING THE ENTIRE LAUE LENS

The method adopted to simulate the PSF of the petal is extended to model the entire lens. The simulation consists of a lens made either with GaAs(220) or with Ge(111) crystal tiles.

The resulting PSF of a lens with pass band from 80 to 600 keV in the case of GaAs (220) is shown in Figs. 7 and 8. Instead, in the case of Ge(111) as the crystal tiles, the resulting PSF is shown in Figs. 9 and 10.

In particular, Fig. 7 (in case of GaAs(220) crystal tiles) and Fig. 9 (in case of Ge(111) crystal tiles) show the PSF in the case of no radial distortion and a perfect positioning of crystal tiles on the lens frame without any misalignment. Instead, Fig. 8 and Fig. 10, respectively, for the case of GaAs(220) and Ge(111), show the PSF when the bent crystal tiles have a large radial distortion of 6 m (from the required 40 m) and are positioned on the petal frame with a maximum misalignment of 30 arcsec.

Parameter	Value	
	case of GaAs(220)	case of Ge(111)
Energy range	80 - 600keV	80 - 600keV
Focal length	20 m	20 m
No. of Rings	45	28
Minimum radius	20.71 cm	12.67 cm
Maximum radius	152.71 cm	93.67 cm
No. of crystal tiles	24494	9341
Crystal dimension	$30 \times 10 \times 2 \text{ mm}^3$	$30 \times 10 \times 2 \text{ mm}^3$
Crystal mass (total)	$2.5 \text{ g} \times 24494 = 61.235 \text{ kg}$	$2.07 \text{ g} \times 9341 = 19.335 \text{ kg}$

Table 3. Parameters of the simulated lens.

The values of the main parameters of the lens are given in Table 3.

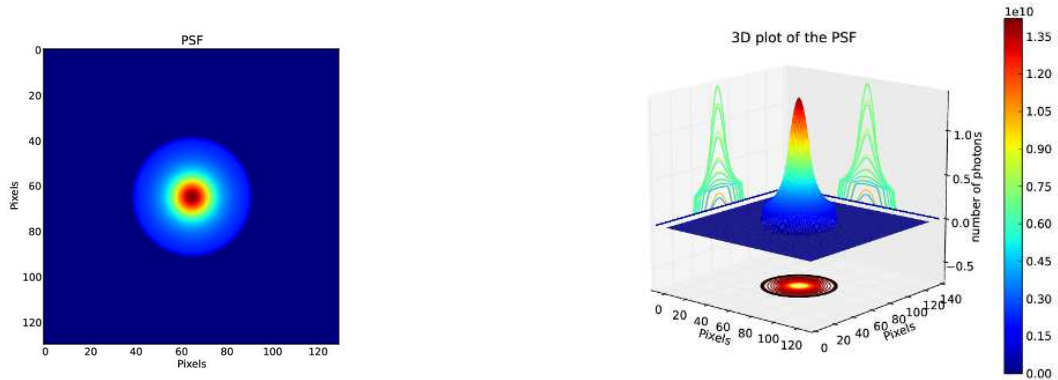


Figure 7. PSF of the lens made with GaAs(220) without any misalignment errors in the positioning of the crystal tiles having no radial distortion.

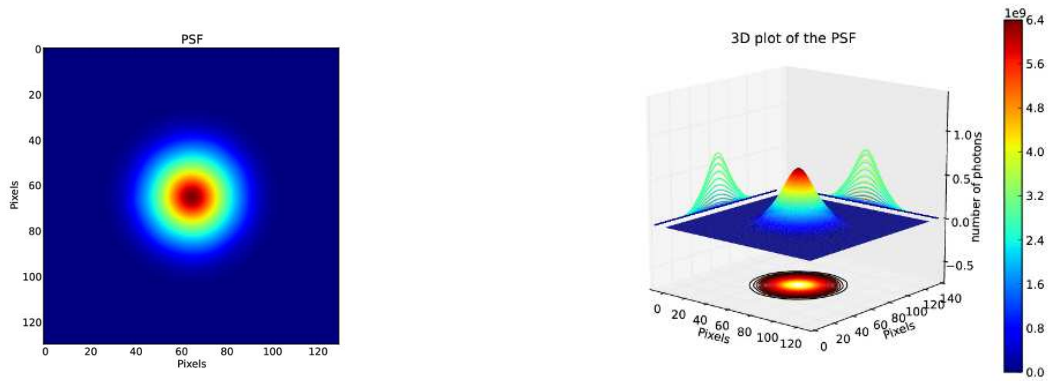


Figure 8. PSF of the lens made with GaAs(220) with a maximum misalignment of 30 arcsec in the positioning of the crystal tiles having a maximum radial distortion of 6 meters.

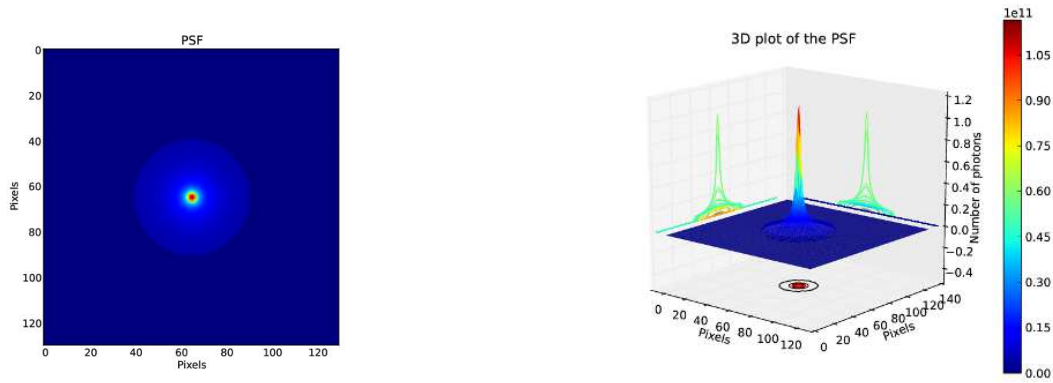


Figure 9. PSF of the lens made with Ge(111) without any misalignment errors in the positioning of the crystal tiles having no radial distortion.

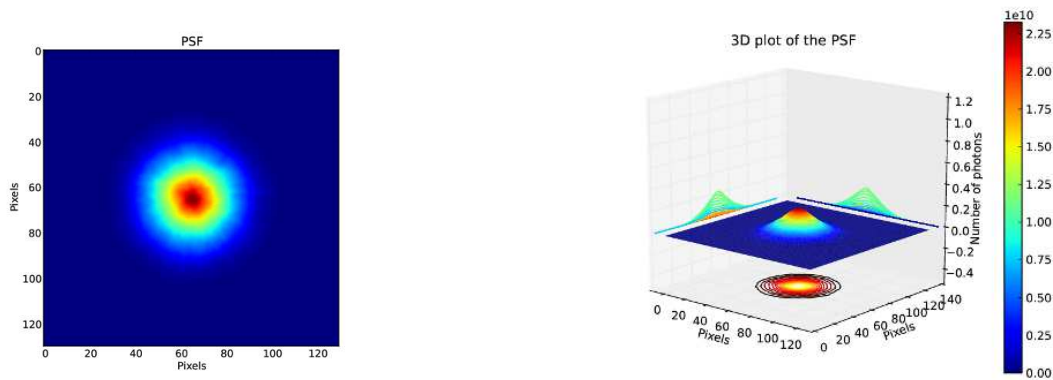


Figure 10. PSF of the lens made with Ge(111) with a maximum misalignment of 30 arcsec in the positioning of the crystal tiles having a maximum radial distortion of 6 meters.

## 5. DISCUSSION

In this section we discuss the lens simulation results in the case of GaAs(220) and Ge(111) crystal tiles, and their consequences.

## 5.1 FWHM profile

Any misalignment in the positioning of the crystal on the lens/petal frame, and also any distortion in the curvature radius will affect the FWHM of the PSF. Fig. 11 shows the dependence of FWHM on the radial distortion for the two lens cases, assuming a perfect positioning of the crystal tiles on the lens frame. As it can be seen, when there is no misalignment and no radial distortion, the FWHM is 3.4 mm in the case of GaAs(220) and 0.6 mm for Ge(111) as the crystal tile used for building the lens.

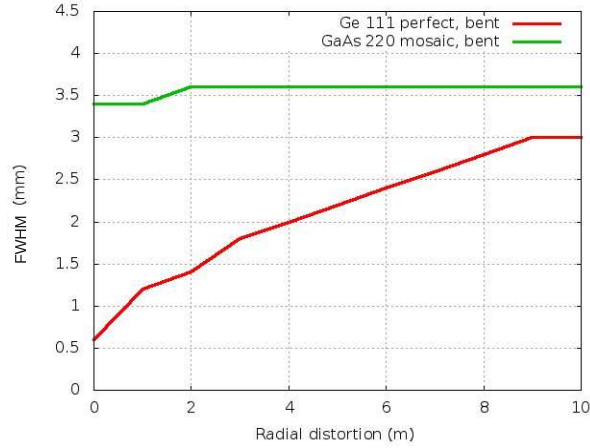


Figure 11. FWHM profile of the lens made with perfect positioning of the crystal tiles on the lens frame.

## 5.2 Peak intensity profile

The effect of misalignment on the peak intensity is plotted in Fig. 12. The peak intensity, as expected, gets reduced with the increase in misalignment error and radial distortion. Assuming 100%, the peak intensity of a lens made by perfect positioning of GaAs(220) crystal tiles and no radial distortion, this value decreases to about 55% for a misalignment (in the positioning of the crystal tile on the lens frame) of 30 arcsec and a large radial distortion of 6 meters. In the case of Ge(111), the corresponding reduction is of about 80%.

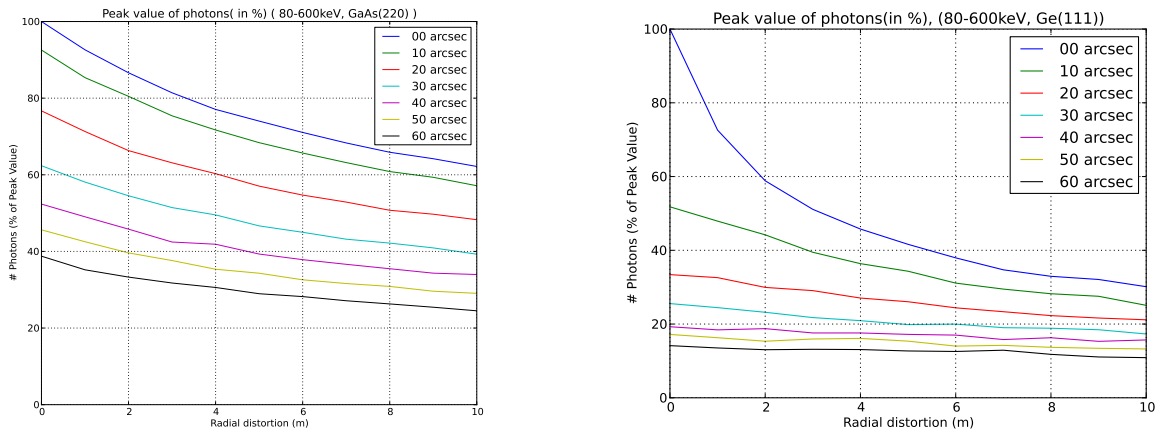


Figure 12. Peak intensity profile of the lens made with GaAs(220) (*left*) and Ge(111) (*right*) for different values of crystal misalignment and radial distortion. The values in the *legend* shows maximum misalignment (in arcsec) in the positioning of crystals.

### 5.3 Radial profile

The radial profile of the PSF is the cumulative distribution of the number of photons collected along the radial distance from the focal point. The PSF of the lens with a perfect alignment (misalignment = 0.0 arcsec [ $M00$ ]) of the crystal tiles and no radial distortion of the bent crystals (radial distortion = 0 meters [ $R0$ ]) is shown in Fig. 13 (case of the lens made by GaAs(220) crystal tiles on the *left* and that of Ge(111) crystal tiles on the *right*).

As it can be seen from the figure, the PSF does not show a ‘Gaussian’ shape, but has at the bottom a ‘trapezoidal’ shape. This shape introduces an offset and increases the background level of the ‘signal’. The normalised radial profiles obtained by subtracting this offset is plotted in Fig. 14. The pixel dimension is  $200 \mu\text{m} \times 200 \mu\text{m}$ .

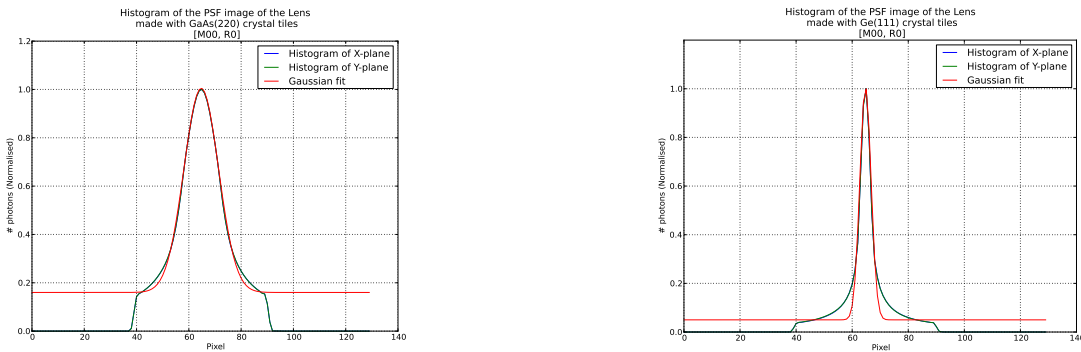


Figure 13. Histogram of the image PSF of the lens made by GaAs(220) crystal tiles (*left*), and that by Ge(111) crystal tiles (*right*). This lens is made with perfect positioning of the crystal tile, having no radial distortions.

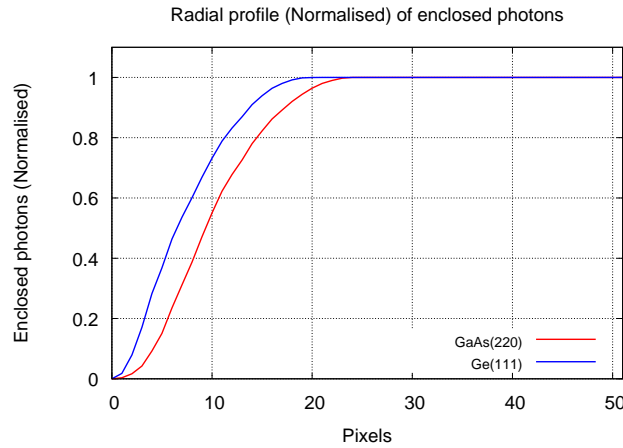


Figure 14. Normalised radial profile of the lens made with perfect positioning of the crystal tile, having no radial distortions. This profile has been calculated by neglecting the ‘trapezoidal’ base of the PSF image.

### 5.4 Effective area

The effective area at an energy  $E$  is the product of the geometrical area of the optics times its reflection efficiency at the same energy  $E$ . When the entire energy range (90-600 keV) of the lens is divided into 10 equal bins (in logarithmic scale), the total geometric area in each bin  $GA_{total}^{bin}$  is taken as the surface area of the lens corresponding to the energy range of each binning.

$$GA_{total}^{bin} = N_c(\Delta E) \times xtal_{area} \quad (1)$$

where  $N_c(\Delta E)$  is the number of crystal tiles associated with the corresponding energy range of the bin, and  $xtal_{area}$  is the surface area of a single crystal tile. The effective area  $Area_{eff}^{bin}$ , in each binning is given by:

$$Area_{eff}^{bin} = GA_{total}^{bin} \times \overline{R_{bin}} \quad (2)$$

where  $R_{bin}$  is the mean reflectivity in each bin.

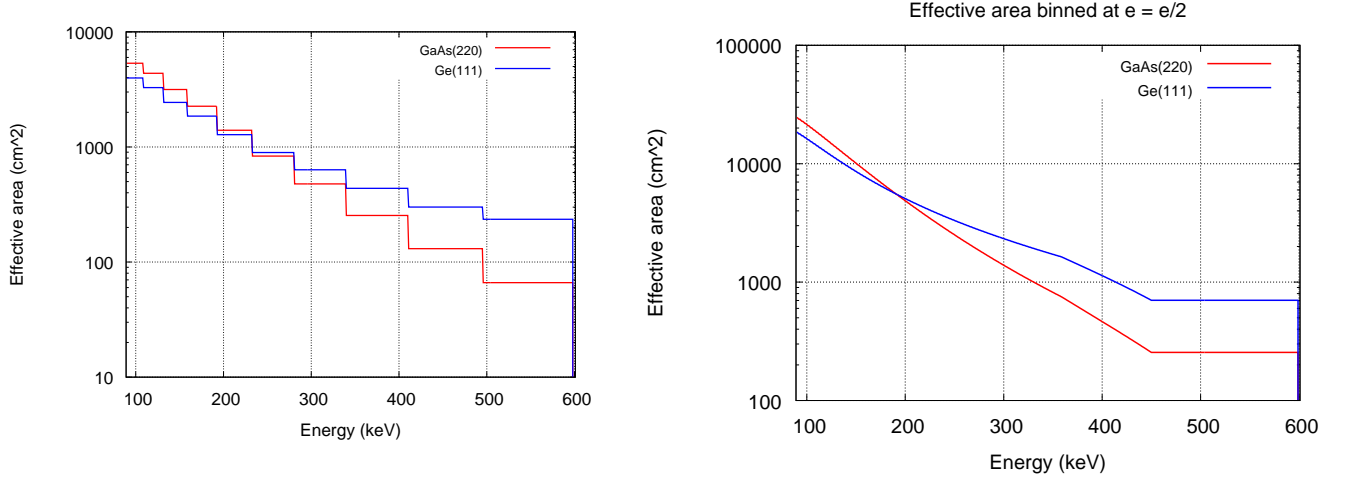


Figure 15. Effective area of the Lens made of GaAs(220) as well as Ge(111) crystal tiles calculated for 10 bins sampled equally in logarithmic scale (*left*) and for  $\Delta E = e/2$  *right*.

Fig. 15 shows the effective area calculated from Eq. 2 in case of GaAs(220) and Ge(111), respectively. The large values of effective area at lower energies and smaller values at higher energies is mainly due to the large difference in the number of crystal tiles corresponding to those energies. For example, the number of Ge(111) crystal tiles corresponding to lowest energy bin are around 2092, but there are only 68 Ge(111) crystal tiles corresponding to the highest energy bin. For lens made with GaAs(220) crystal tiles there are 5580 tiles for the lowest energy bin and 182 tiles for the highest energy bin.

## 5.5 Continuum sensitivity

Sensitivity of a telescope is defined as the minimum intensity,  $I_s^{min}$  which can be "detected" by the detector in an observation time  $T_{obs}$ . For a focusing telescope, if the total noise measured is only due to the background (the noise due the source is negligible), the sensitivity,  $I_{ft}^{min}(E)$  is given by:

$$I_{ft}^{min}(E) = n_\sigma \frac{\sqrt{B(E)}\sqrt{A_d}}{\eta_d f_\epsilon A_{eff} \sqrt{\Delta E} \sqrt{T_{obs}}} \quad (3)$$

where,

- $n_\sigma$  is the confidence level (usually  $3\sigma$ );
- $B(E)$  is the intensity of the measured background spectrum (in *counts/s/cm²/keV*) at the energy  $E$ ;
- $\eta_d$  is the efficiency of the position sensitive detector;
- $A_d (= \pi R_{spot}^2)$  is the detector area covered by the incoming photons within a radius of  $R_{spot}$ ;
- $\Delta E$  is the energy band around  $E$ ;
- $T_{obs}$  is the observation time;

- $f_\epsilon$  is the fraction of photons that is incident on the detector area  $A_d$ ;
- $A_{eff}$  is the effective area at an energy  $E$  of the telescope optics, given by the product of the geometrical area of the optics times its reflection efficiency at that energy  $E$ .

Figure 16 shows the  $3\sigma$  sensitivity for an observation time of  $10^5$  s and  $10^6$  s, along with  $\Delta E = E/2$  and background =  $1.5 \times 10^{-4}$  counts/sec/cm<sup>2</sup>/keV.

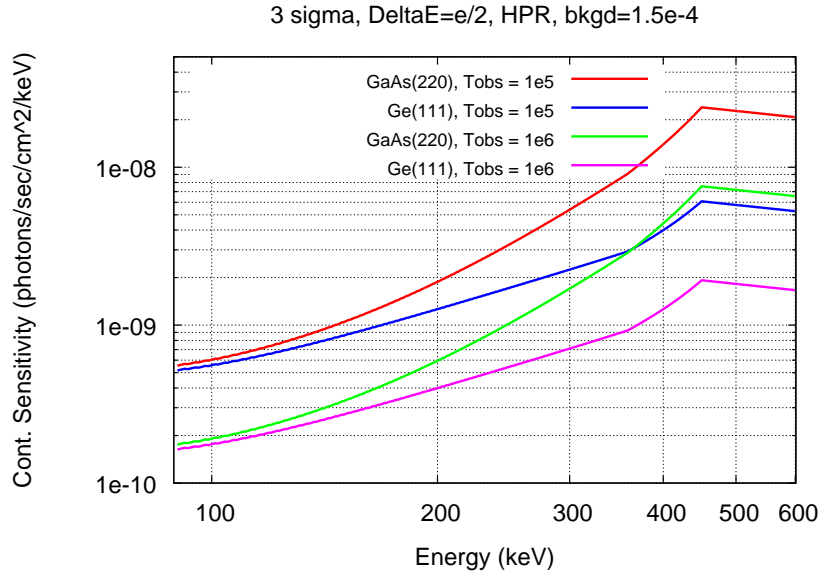


Figure 16.  $3\sigma$  Continuum sensitivity of the Lens with time of observation  $10^5$  seconds and  $10^6$  seconds with  $\Delta E = e/2$ , background =  $1.5 \times 10^{-4}$  and  $R_{spot} = \text{HPR}$

## 5.6 Line sensitivity

The line sensitivity can be obtained from the continuum sensitivity by superposing an emission line to the continuum intensity. In the case of a focusing telescope, if the source continuum level can be accurately determined, the minimum detectable intensity  $I_L^{min}$  (in photons/s/cm<sup>2</sup>), of a line is given by

$$I_L^{min}(E_L) = 1.31n_\sigma \frac{\sqrt{[2B(E_L)A_d + I_c(E_L)\eta_d f_\epsilon A_{eff}]\Delta E}}{\eta_d f_\epsilon A_{eff} \sqrt{T_{obs}}} \quad (4)$$

where,

- $n_\sigma$  is the confidence level (usually  $3\sigma$ );
- $B(E_L)$  is the intensity of the measured background spectrum (in counts/s/cm<sup>2</sup>/keV) at the energy  $E_L$ ;
- $A_d (= \pi R_{spot}^2)$  is the detector area covered by the incoming photons within a radius of  $R_{spot}$ ;
- $I_c(E_L)$  is the intensity (in counts/s/cm<sup>2</sup>/keV) at the continuum of the source at the centroid of the line;
- $\eta_d$  is the efficiency of the position sensitive detector;
- $f_\epsilon$  is the fraction of photons that is incident on the detector area  $A_d$ ;
- $\Delta E$  is the FWHM around  $E_L$ . This value depends upon the energy resolution of the detector;

- $T_{obs}$  is the observation time;
- $A_{eff}$  is the effective area at an energy  $E_L$  of the telescope optics, given by the product of the geometrical area of the optics times its reflection efficiency at that energy  $E_L$ .

The line sensitivity for the lens made with perfectly positioned GaAs(220) or Ge(111) bent crystal tiles with no radial distortion, is shown in Fig. 17. The sensitivity of each lens is plotted separately for  $10^5$  s and  $10^6$  s observation time. The values of other parameters are the following:  $n_\sigma = 3$ ,  $A_d$  is the area corresponding to half power radius (for  $f_\epsilon = 50\%$  of enclosed photons)  $\eta_d = 90\%$ ,  $\Delta E = 2$  keV, which is the energy resolution of the CZT detector intended for our use, and finally  $A_{eff}$  corresponds to the data from Fig. 15 with a filling factor of 0.2 mm.

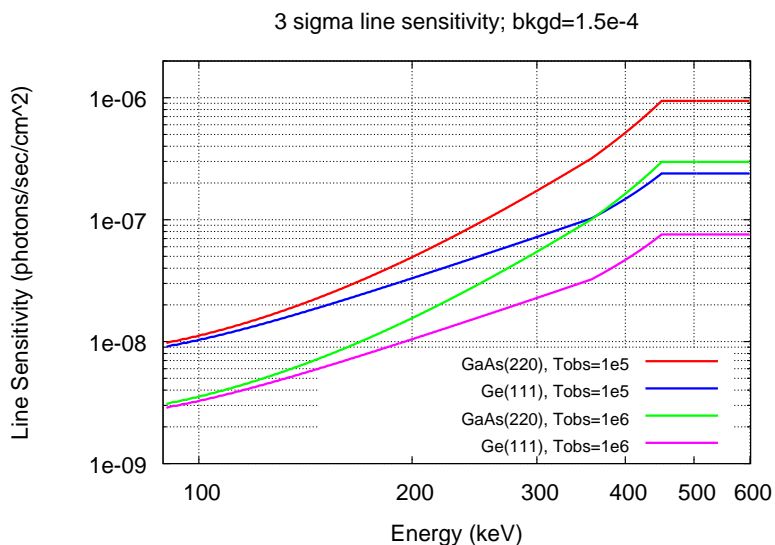


Figure 17. Line sensitivity of the lens.

## 6. CONCLUSION

We have presented the performance of a simulated lens petal and of a lens made of either GaAs(220) or Ge(111) crystal tiles. The effect of divergence of the beam on the petal PSF has been simulated. The dimension of the diffracted image of GaAs(220) crystal tile glued on the petal structure is found to be similar to that calculated through simulation, including the divergence. The divergence of the beam is a significant factor affecting the PSF.

Energy (keV)	Simulation ( $T_{obs} = 10^5$ s)		ISGRI	SPI
	GaAs(220)	Ge(111)	$T_{obs}=10^5$ s	$T_{obs}=10^6$ s
100	$6.04 \times 10^{-10}$	$5.57 \times 10^{-10}$	$2.85 \times 10^{-6}$	$7.0 \times 10^{-6}$
500	$2.24 \times 10^{-8}$	$5.76 \times 10^{-9}$	$9.83 \times 10^{-6}$	$1.5 \times 10^{-6}$

Table 4. Comparison of the  $3\sigma$  continuum sensitivity (in photons/sec/cm<sup>2</sup>/keV) of simulated lens with ISGRI and SPI on-board INTEGRAL.

The simulation of the petal has been extended to model an entire lens made of petals. The effective area, the continuum sensitivity as well as the line sensitivity are calculated. These results show that this lens is about 3 orders of magnitude more sensitive (see Table 4) than ISGRI<sup>13</sup> and SPI<sup>14</sup> on-board INTEGRAL satellite.

## ACKNOWLEDGMENTS

The authors wish acknowledge the financial support by the Italian Space Agency (ASI) through the project “LAUE: Una lente per i raggi Gamma” Under contract I/068/09/0. Vineeth Valsan and Vincenzo Liccardo are supported by the Erasmus Mundus Joint Doctorate Program by Grant Number 2010-1816 from the EACEA of the European Commission.

## REFERENCES

- [1] Frontera, F., Virgilli, E., Liccardo, V., Valsan, V., Carassiti, V., Chiozzi, S., Evangelisti, F., Squerzanti, S., Statera, M., Guidi, V., Ferrari, C., Zappattini, R. A., Caroli, E., Auricchio, N., Silvestri, S., Camattari, R., Cassase, F., Recanatesi, L., Pecora, M., S.Mottini, and Negri, B., “Development status of laue project,” *SPIE Conference Series* **8443** (2012).
- [2] Frontera, F., Virgilli, E., Valsan, V., Liccardo, V., Carassiti, V., Caroli, E., Cassase, F., Ferrari, L. R. C., Guidi, V., Pecora, M., S.Mottini, Amati, L., Auricchio, N., Bassani, L., Campana, R., Farinelli, R., Guidorzi, C., Labanti, C., Landi, R., Malizia, A., Orlandini, M., Sguera, V., Stephen, J. B., and Titarchuk, L. G., “Scientific prospects in soft gamma-ray astronomy thanks to the laue project,” *SPIE Conference Series* **8861** (2013).
- [3] Frontera, F. and Ballmoos, P. V., “Laue gamma-ray lenses for space astrophysics: status and prospects,” *astro-ph.IM* (2011).
- [4] Loffredo, G., Frontera, F., Pellicciotta, D., Pisa, A., Carassiti, V., Chiozzi, S., Evangelisti, F., Landi, L., Melchiorri, M., and Squerzanti, S., “The ferrara hard x-ray facility for testing/calibrating hard x-ray focusing telescopes,” *Experimental Astronomy* **20**, 413–420 (Dec. 2005).
- [5] Virgilli, E., Frontera, F., Valsan, V., Liccardo, V., Carassiti, V., Evangelisti, F., and Squerzanti, S., “Laue lenses for hard x/soft gamma rays: new prototype results,” *SPIE Conference Series* **8147** (2011).
- [6] Frontera, F., Loffredo, G., Pisa, A., Nobili, F., Carassiti, V., Evangelisti, F., Landi, L., Squerzanti, S., Caroli, E., Stephen, J. B., Anderson, K. H., Courtois, P., Auricchio, N., Milani, L., and Negri, B., “Focusing of gamma-rays with laue lenses: first results,” in [*Society of Photo-Optical Instrumentation Engineers (SPIE) Conference Series*], 7011, SPIE (2008).
- [7] Ferrari, F., Frontera, F., Loffredo, G., Virgilli, E., Guidorzi, C., Carassiti, V., Evangelisti, F., Landi, L., Chiozzi, S., Squerzanti, S., Caroli, E., Stephen, J. B., Shiavonne, F., Basili, A., Andersen, K. H., and Courtois, P., “New results on focusing of gamma rays with laue lenses,” in [*Optics for EUV, X-Ray, and Gamma-Ray Astronomy III*], *Proceedings of the SPIE* **7437-19**, Presented at the Society of Photo-Optical Instrumentation Engineers (SPIE) Conference (2009).
- [8] Frontera, F., Loffredo, G., Pisa, A., Milani, L., Nobili, F., Auricchio, N., Carassiti, V., Evangelisti, F., Landi, L., Squerzanti, S., Andersen, K. H., Courtois, P., Amati, L., Caroli, E., Landini, G., Silvestri, S., Stephen, J. B., Poulsen, J. M., Negri, B., and Pareschi, G., “Development status of a laue lens project for gamma-ray astronomy,” in [*Optics for EUV, X-Ray, and Gamma-Ray Astronomy III*], O’Dell, S. L. and Pareschi, G., eds., *Proceedings of the SPIE* **20**, 6688, Presented at the Society of Photo-Optical Instrumentation Engineers (SPIE) Conference (2007).
- [9] Valsan, V., Frontera, F., Virgilli, E., and Liccardo, V., “Expected performance of a laue lens based on bent crystals,” *SPIE Conference Series* **8443** (2012).
- [10] Liccardo, V., Frontera, F., Virgilli, E., Valsan, V., Guidi, V., and Ferrari, C., “Bent crystal selection and assembling for the laue project,” *SPIE Conference Series* **8861** (2013).
- [11] Virgilli, E., Frontera, F., Valsan, V., Liccardo, V., Carassiti, V., Evangelisti, F., Squerzanti, S., Parise, M., Statera, M., v. Guidi, , Bellucci, V., Camattari, R., Caroli, E., Auricchio, N., Basili, A., Silvestri, S., Stephen, J. B., Cassese, F., Recanatesi, L., Ferrari, C., Zappettini, A., Buffagni, E., Mottini, S., Pecora, M., and Negri, B., “The laue project and its main results,” *SPIE Conference Series* **8861** (2013).
- [12] Liccardo, V., Frontera, F., Virgilli, E., and Valsan, V., “Characterization of bent crystals for laue lenses,” *SPIE Conference Series* **8443** (2012).
- [13] Blanger, G., *INTEGRAL IBIS Observers Manual*. ESA, 1.0 ed. (March 2012).
- [14] Fernandez, C. S., *INTEGRAL SPI Observers Manual*. ESA, 1.0 ed. (March 2012).